Tribology and Materials
Vol. 4, No. 2, 2025, pp. 90-99

ISSN 2812-9717
https://doi.org/10.46793/tribomat.2025.011

Power losses vs. mechanical load of an active magnetic bearing: A finite element method approach

**Vasileios Menelaos KOUFOPANOS , Andreas ANDRIKOPOULOS , Pantelis NIKOLAKOPOULOS *

University of Patras, Patras, Greece
*Corresponding author: pnikolakop@upatras.gr

Keywords

active magnetic bearings
ohmic losses
iron losses
mechanical load capacity
finite element method

History

Received: 20-10-2024
Revised: 31-01-2025
Accepted: 03-03-2025

Abstract

Active magnetic bearings are a novel solution for supporting rotating shafts. Thanks to the electromagnets and their ability to apply forces without any mechanical contact needed, they enable frictionless rotation while eliminating wear. Although mechanical friction is absent in such an element, there are other loss mechanisms to consider, such as the ohmic losses on each electromagnet's coils, as well as the iron losses caused by the alternating magnetic field on the rotor and, occasionally, on the stator. In this paper, the effects of the bearing's length, the air gap and the bias current, both on the bearing's mechanical load capacity and on the ohmic and iron losses, are examined. A series of values for the aforementioned parameters is tested using a 2D finite element transient model, which calculates the bearing's mechanical load and iron losses, in addition to analytical calculations for the ohmic losses. Then, the control current required for a specific mechanical load is calculated for different bearing lengths and magnetic air gaps. Considering the ohmic and iron losses for each case, a value for the air gap and the bearing's length is selected to achieve the required load while the losses are minimised.

1. Introduction

The friction between a bearing and its rotor is one of the most common issues tribology deals with, as this tribosystem is a considerable source of power loss for rotating machinery. While much progress has been achieved regarding roller [1] and journal bearings [2], research also deals with more modern bearing types. Active magnetic bearings (AMBs) have become very popular over the last few decades, as they can provide contactless rotation by means of magnetic forces applied by the stator's electromagnets to the rotor's ferromagnetic part. As a result, friction losses and wear are eliminated [3]. Their applications include but are not limited to, high-speed rotors for machine tools [4], flywheels [5] and turbomolecular pumps [6].

Due to the applications mentioned above, the vast majority of research related to AMBs deals with feedback control strategies [7], high-speed rotor levitation [8] and challenges related to vacuum, especially the dissipation of the heat occurring due to the AMB's operation [9-11]. Fault detection and condition monitoring are also frequently addressed. A review on vibration suspension and condition monitoring novelties related to AMBs and flexible rotors was published by Siva Srinivas et al. [12]. There is also an increasing trend of developing digital twin models of AMB systems for fault detection and optimised performance [13,14]. Those applications require adequate and detailed simulation models in the first place.

Power losses appear in such devices, not only because of the electric current the electromagnets require but also because of the alternating magnetic field caused by the shaft's rotational motion and the electric currents' fluctuation. Those two loss mechanisms are known as ohmic or copper losses and iron losses, respectively, and they are an essential factor in an AMB's design process.

Ohmic losses occur due to the electric current flow in the coils' windings, and they are proportional to the electric current (squared) and the ohmic resistance of the wire. Those losses also occur at the power supply system and its cables, yet this paper only focuses on the AMB's stator and rotor, neglecting this part of the losses. Iron losses can be divided into two main categories according to Maslen and Schweitzer [3]: the hysteresis losses, which appear due to the hysteresis in the magnetisation of the magnetic core (i.e. the stator and the rotor's ferromagnetic material in this case), as well as the eddy current losses. The latter refers to electric currents occurring due to the alternating magnetic field inside the ferromagnetic core, which creates a magnetic flux that opposes the desired one. The alternation of the field is mainly due to the shaft's rotation but also due to the current fluctuation at the stator's coils.

The calculation of an AMB's ohmic and iron losses can be achieved either by using analytical methods or finite element models and experimental devices. Xu et al. [9] calculated the AMB losses for a turbomolecular pump, considering the temperature's influence. While they obtained the magnetic field solution using finite element method (FEM), they used the magnetic flux density values for some key points of the geometry and analytical methods in order to calculate the iron losses of the bearing, validating the results experimentally. A similar work is presented by Zhang et al. [10], including DC bias magnetisation effects on the iron losses. Thermal effects on iron loss are also addressed by Han et al. [11].

While the aforementioned works are based on magnetostatic and/or eddy current FEM solutions, Santra et al. [15] perform FEM analysis to address the losses occurring because of the magnetic field rotation for two passive radials and an active thrust magnetic bearing. Koufopanos and Nikolakopoulos [16] used a FEM transient model to calculate the iron losses of AMBs, comparing three different iron-cobalt alloys. Li et al. [17] explore the effects of eddy currents on the performance of the switching power amplifier using simulation and experimental methods. Several multi-objective optimisation approaches regarding the AMB's geometry and power losses have also been recently published, showing the current research trend [18-21].

The main goal of this paper is to correlate the two power loss types, ohmic and iron, with AMB's geometry parameters, its length and air gap, as well as the (constant) bias current provided to the coils. This is achieved by means of FEM, using a 2D transient magnetic model of the AMB, which calculates the two components of the iron losses that occur as a result of the rotor's motion inside the bearing's stator, in addition to the AMB's mechanical load. The calculations are performed for a range of length, air gap and bias current values. The ohmic losses for those cases are also calculated using analytic equations. Then, for a specific mechanical load of 40 N, the required control current for different AMB lengths and air gaps is calculated, in addition to the power losses, so that the optimum set of values regarding energy consumption is selected.

The novelty of this approach is the modelling, using FEM, of the rotor's motion inside the stator of the AMB instead of the electric current's fluctuation in the stator's coils which is usually addressed. The advantage of FEM over analytical methods relies on the more accurate solution of the magnetic field distribution on the studied geometry, including flux leakage and skin effects as well. The flux density distribution plays a significant role in the iron loss calculation [22,23]. The model has already been validated based on results already published in the literature. The validation process has already been described by Koufopanos and Nikolakopoulos [16].

2. Finite element model of the AMB – rotor system

The finite element model used for this analysis is created using the Ansys Maxwell software. The rotor's motion is simulated at a specific speed for an adequate runtime, and the magnetic flux density distribution is derived for the selected time steps. The advantage of FEM compared to analytical methods is that the distribution of the flux is more accurately calculated in the stator's and the rotor's interior, leading to more accurate results regarding the magnetic force applied on the rotor and the iron losses.

The geometry of an 8-pole radial heteropolar AMB, as it was created in the software, can be seen in Figure 1. A grey colour represents the ferromagnetic material, while a bronze colour represents the coils, made of copper. The current of each winding is defined as "stranded" and is equal to the sum of the bias and the control component ($I_b \pm I_c$). The bias current remains constant, while the control current is responsible for the creation of the magnetic force on each electromagnet pair. The surrounding is considered to be a vacuum. As a boundary condition, a square box surrounding the geometry is created slightly bigger than the AMB's stator. At the square's edges, the magnetic flux is set to 0 Wb. The calculations provide results per unit length since the geometry is 2D, but the length of the AMB can be input so that a 3D approximation is available. For the mesh, the software uses 2D triangular elements, while the finest mesh operation setting was selected for the curved surfaces. The transient solution simulates 100 rotations of the shaft, with each rotation discretized in 8 steps.

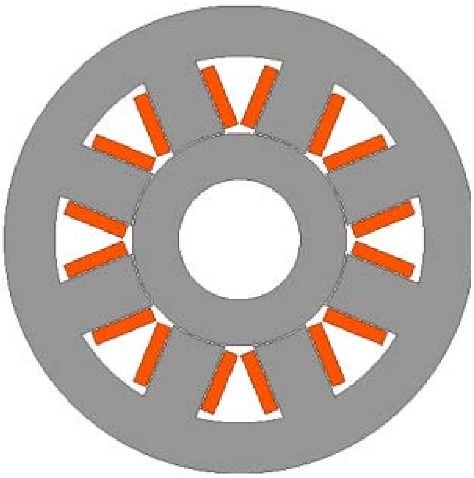

Figure 1. AMB geometry in ANSYS Maxwell environment

The main input of the model is the electric current, which is provided to the coils. The current is considered constant throughout the simulation, which means that any alterations because of the power amplifier and the controller are neglected. The coils of the upper and lower magnets, which are responsible for the vertical magnetic force, have a (constant) control current component, which is necessary for the support of the rotor's weight. The horizontal magnetic force is considered zero, hence no control current is needed on the respective coils. The rotor part is defined as a component with a constant rotational speed attributed to it, while any vibrating motion is neglected. The ferromagnetic material used in this analysis is a 3 % grain-oriented silicon steel, a soft ferromagnetic alloy that is made by adding 3 wt. % silicon to iron in order to enhance its magnetic properties. The alloy is used in the form of laminated sheets (0.356 mm). The electric conductivity of the alloy is 2,500,000 S/m. The BH curve (magnetisation curve) [24], as well as the BP curve (iron loss as a function of the magnetic induction), are imported [25].

The 2D transient solver of the model is based on the calculation of magnetic vector potential $\boldsymbol{A}$ and the electric potential φ, using the electric current density $\boldsymbol{J}$ of the defined conductors as input, as well as other parameters referring to the materials' properties, such as the magnetic permeability μ, the electric conductivity σ and the magnetic coercivity H_C [26]. This problem is solved for several time-steps, with each step considering as initial conditions the results of the previous one, in addition to the, so far, rotational displacement of the rotor part.

Each solution step begins with the electric current density calculation by summing the input currents defined by the user to the eddy currents induced by the rotor's motion. Then, through an iterative process, the new magnetic vector potential A is calculated for each node using the following equation [26]:

$$\nabla \times \frac{1}{\mu} \nabla \times \boldsymbol{A} = \boldsymbol{J}_\mathrm{s} - \boldsymbol{J}_\mathrm{in} + \nabla \times H_\mathrm{C}, \tag{1}$$

where $\boldsymbol{J}_\mathrm{s}$ is the source electric current density of the coils and $\boldsymbol{J}_\mathrm{in}$ is the induced electric current density because of the field's alternation. This equation is a variation of Ampere's law [27]:

$$\nabla \times \boldsymbol{H} = \boldsymbol{J}. \tag{2}$$

Considering the magnetic flux density as $\boldsymbol{B} = \mu H$ and replacing it with the definition of the magnetic vector potential $\boldsymbol{A}$:

$$\nabla \times \boldsymbol{A} = \boldsymbol{B}. \tag{3}$$

The induced electric current density is derived from a variation of Faraday's law:

$$\boldsymbol{E}_\mathrm{in} = -\nabla \varphi - \frac{\mathrm{d}\boldsymbol{A}}{\mathrm{d}t}, \tag{4}$$

where $\boldsymbol{E}_\mathrm{in}$ is the induced electric field intensity.

Considering $\boldsymbol{J} = \sigma \boldsymbol{E}$, it could be written as:

$$\boldsymbol{J}_\mathrm{in} = -\sigma \nabla \varphi - \sigma \frac{\mathrm{d}\boldsymbol{A}}{\mathrm{d}t}. \tag{5}$$

The term $\mathrm{d}\boldsymbol{A}/\mathrm{d}t$ stands for the magnetic vector potential change inside the material because of its motion.

The above process is performed in every loop so that the magnetic flux density $\boldsymbol{B}$ is obtained for each node considering the nonlinear magnetisation behaviour of the material. The attractive magnetic force of each pole applied on the rotor is calculated by the formula [3]:

$$\boldsymbol{F} = \frac{\boldsymbol{B}^2 \boldsymbol{A}}{\mu_0}. \tag{6}$$

This method provides a more accurate solution for the magnetic force than the linearised equation, which considers a linear relationship between magnetic flux density and electric current [3]:

$$F_{\mathrm{mag}} = k_{\mathrm{i}} I_{\mathrm{C}} - k_{\mathrm{s}} x, \tag{7}$$

where x is the rotor's displacement and k_{i} and k_{s} are stiffness factors for the electric current and the displacement, respectively.

The model then calculates the iron losses (per volume unit) P_{iron}, using the following equation, which is a modified version of the iron loss separation equation [26]:

$$P_{\mathrm{iron}} = P_{\mathrm{hyst}} + P_{\mathrm{ec}} = C_{\mathrm{dc}} k_{\mathrm{h}} f B^2 + k_{\mathrm{e}} f^2 B^2, \tag{8}$$

where P_{hyst} is the hysteresis loss component, P_{ec} is the eddy currents loss, B is the magnitude of the magnetic flux density alternation, f is the magnetisation frequency, k_{e} and k_{h} are the eddy current and hysteresis loss factors, respectively (derived from the material's BP curve) and C_{dc} is the dc-biased hysteresis loss parameter (used when the magnetic field alternates around a non-zero value making the magnetisation loop asymmetric).

As for the ohmic losses P_{ohmic} for each one of the eight windings, they are the product of the current's square I^2 with the wire's ohmic resistance R:

$$P_{\mathrm{ohmic}} = I^2 R. \tag{9}$$

The ohmic resistance of the wire depends on its geometry, as well as the resistivity ρ of the copper:

$$R = \frac{\rho l}{A_{\mathrm{wire}}}, \tag{10}$$

where l is the length of each wire and A_{wire} is its cross-section area.

For the first part of this analysis, an AMB is modelled for a range of values for its length, air gap and the supplied bias current. The input parameters of the model that remain constant are listed in Table 1. The elements for the mesh varied based on the air gap value since this part of the geometry needed the finest mesh possible. For the smallest air gap case (0.275 mm), the elements were 12,534, while for the largest one (0.605), 12,220 triangles were used.

Table 1. Input parameters for the AMB – rotor model (Test 1)

Parameter	Value
Stator's outer diameter	164 mm
Stator's inner diameter	127 mm
Coil turns per pole	100
Pole width	18 mm
Rotational speed	30,000 rpm
Lamination thickness	0.356 mm
Control current (y-direction)	0.5 A

In Table 2, all the parameter combinations examined in this part of the analysis are listed. For constant air gap and bias current values, the AMB's length varies from 30 to 60 mm. Similarly, for a constant length and bias current, the air gap ranges from 0.275 to 0.605 mm. This is achieved by changing the diameter of the rotor each time while keeping the same stator. Thirdly, the bias current values are checked within the 0.5 to 2.5 A range for a constant AMB length and magnetic air gap. For each set of values, ohmic and iron losses are calculated, in addition to the magnetic force. Those results will indicate the impact of each parameter on the AMB's energy consumption and effectiveness.

Table 2. Tested values of AMB's length, magnetic air gap, rotor's diameter and bias current (Test 1)

<table>
<tr><th>AMB's length, mm</th><th>Magnetic air gap, mm</th><th>Rotor's diameter, mm</th><th>Bias current, A</th></tr>
<tr><td>30.0</td><td rowspan="5">0.440</td><td rowspan="5">46.500</td><td rowspan="5">1.5</td></tr>
<tr><td>37.5</td></tr>
<tr><td>45.0</td></tr>
<tr><td>52.5</td></tr>
<tr><td>60.0</td></tr>
<tr><td rowspan="7">45.0</td><td>0.275</td><td>46.665</td><td rowspan="7">1.5</td></tr>
<tr><td>0.330</td><td>46.610</td></tr>
<tr><td>0.385</td><td>46.555</td></tr>
<tr><td>0.440</td><td>46.500</td></tr>
<tr><td>0.495</td><td>46.445</td></tr>
<tr><td>0.550</td><td>46.390</td></tr>
<tr><td>0.605</td><td>46.335</td></tr>
<tr><td rowspan="5">45.0</td><td rowspan="5">0.440</td><td rowspan="5">46.500</td><td>0.5</td></tr>
<tr><td>1.0</td></tr>
<tr><td>1.5</td></tr>
<tr><td>2.0</td></tr>
<tr><td>2.5</td></tr>
</table>

In the second part of the analysis, a value of 40 N is requested for the magnetic force, assuming that a rotor of this specific load needs to be carried. For a constant bias current, different air gaps and AMB lengths are tested within the ranges of 0.33 – 0.55 mm and 37.5 – 60 mm, respectively. The control current required for the magnets in the vertical direction in order to support this specific static load is found for each case, and the occurring losses are calculated. Dynamic loads, hence, any dynamic control current alternations are neglected in this analysis. The goal is to find the optimum geometry in terms of losses among the ones that produce the same magnetic force. The input parameters for the model are listed in Table 3, followed by the air gap and length parameters to be tested in Table 4. The element number, in this case, varied from 12,252 triangles for the 0.55 mm air gaps to 12,420 for the 0.33 mm air gaps.

Table 3. Input parameters for the AMB – rotor model (Test 2)

Parameter	Value
Stator's outer diameter	164 mm
Stator's inner diameter	127 mm
Coil turns per pole	500
Pole width	18 mm
Rotational speed	30,000 rpm
Lamination thickness	0.356 mm
Bias current	1 A

The results are presented in graphs and tables in the following section. It should be noted that the ohmic component of the losses is calculated analytically using Equations (9) and (10). The model uses Equations (1) to (5) to calculate the magnetic flux distribution numerically and then proceeds to the magnetic force and iron loss calculation using Equations (6) and (8), respectively.

3. Results and discussion

3.1 Effect of length, air gap and bias current on AMB's power loss and magnetic force (Test 1)

For Test 1, magnetic force and power losses were calculated and plotted for several length, air gap and bias current values. Starting with the AMB's length and a value range between 30 and 60 mm (while the air gap and bias current remain constant), the magnetic force applied on the rotor

Table 4. Tested values of magnetic air gap, rotor's diameter and AMB's length (Test 2)

Magnetic air gap, mm	Rotor's diameter, mm	AMB's length, mm
0.330	46.610	37.5
		45.0
		52.5
		60.0
0.385	46.555	37.5
		45.0
		52.5
		60.0
0.440	46.500	37.5
		45.0
		52.5
		60.0
0.495	46.445	37.5
		45.0
		52.5
		60.0
0.550	46.390	37.5
		45.0
		52.5
		60.0

shows a well-expected behaviour, i.e. an increase in length leads to higher mechanical load capacity (Fig. 2). The linear behaviour between the magnetic force and the bearing's length is verified since the force is linearly proportional to the pole's face area. The power losses increase as well (Fig. 3). The ohmic/copper component of the losses increases with AMB's length because the coil's wire becomes longer, leading to higher ohmic resistance. At the same time, the volume of the stator and the ferromagnetic part of the rotor increase and hence, the iron losses become higher. Eddy current loss mechanism (red curve) seems to be the most dominant one. The answer to whether an AMB of a bigger length is more efficient in terms of mechanical load capacity compared to power consumption (as they both increase with length) is provided by the results of Test 2.

The next parameter to be checked is the magnetic air gap. By keeping the stator's geometry constant and varying the rotor's diameter between 46.335 and 46.665 mm, the air gap eventually varies from 0.275 to 0.605 mm (Table 2). As the air gap becomes bigger, the force decreases in a nonlinear way, as can be seen in Figure 4. When it comes to power losses, they show an overall decreasing behaviour (Fig. 5), with a few inconsistencies spotted for some air gap values. The reason is that the decrease of the air gap value is very small in each step, in addition to minor computational errors, as the air gap area is very small compared to the overall geometry, making the calculations very sensitive. While the ohmic component of the losses remains constant, as nothing related to the coil's wire or the electric current changes, the iron losses and especially the eddy currents, decrease in bigger air gaps. Given that a bigger air gap negatively affects the magnetic flux density in the ferromagnetic material, it results in lower mechanical load but also lower power loss. This leads to the need for higher electric currents when the air gap increases. So, the question of whether a bigger air gap is a solution that increases effectiveness alongside energy consumption will be answered in Test 2.

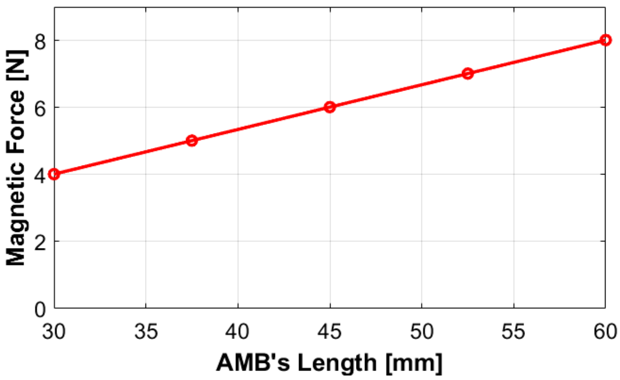

Figure 2. Magnetic force vs. AMB's length

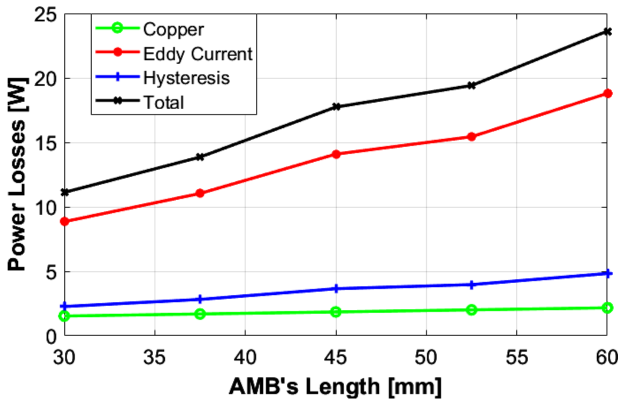

Figure 3. Power losses vs. AMB's length

Lastly, the effect of bias current on the magnetic force and the power losses was tested. While keeping the control current in the vertical direction constant at 0.5 A, the bias current was tested within the range of 0.5 to 2.5 A. One could expect that the magnetic force F_{mag} would remain constant since the control current I_c does not change, based on the linearised magnetic force equation (Equation 7). This equation, however, neglects the nonlinear magnetic behaviour of the ferromagnetic material, which is quite apparent in the case of a constantly alternating field.

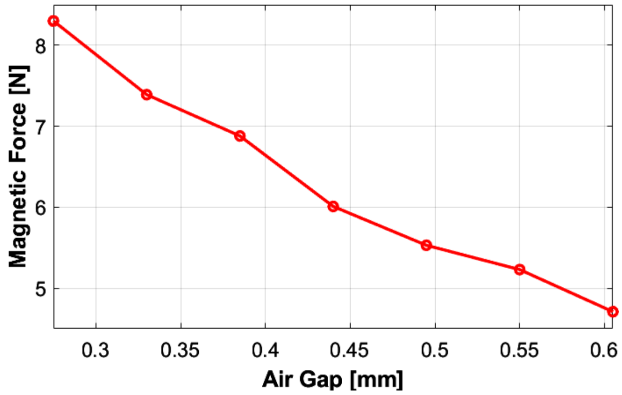

Figure 4. Magnetic force vs. air gap

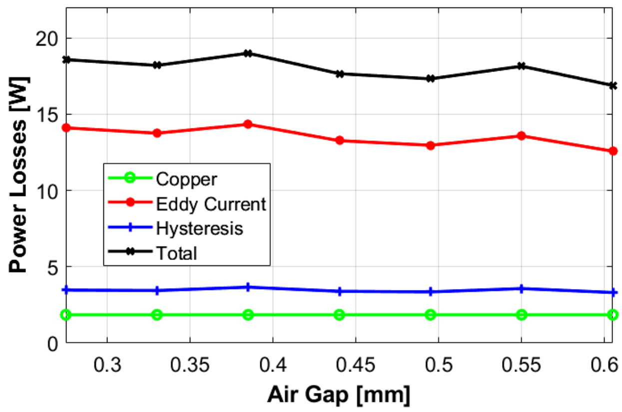

Figure 5. Power losses vs. magnetic air gap

Figure 6 shows that for very low bias current values, the magnetic force is significantly lower compared to higher bias currents, even if the control current is the same. However, as the bias current increases, the force tends to reach a constant value. It seems that when the bias current I_b is very low and almost equal to the control current I_c, the lower magnet's total current ($I_b - I_c$) tends to be near zero. This means that the part of the rotor that "faces" this magnet at the time might fail to adjust the magnetic flux in its interior, accordingly, leading to a non-desired behaviour of the specific magnetic circuit and, as a result, to a magnetic force lower than expected. The conclusion is that the AMB's coils need to operate on a bias current significantly higher than the control current so that they can provide robust behaviour.

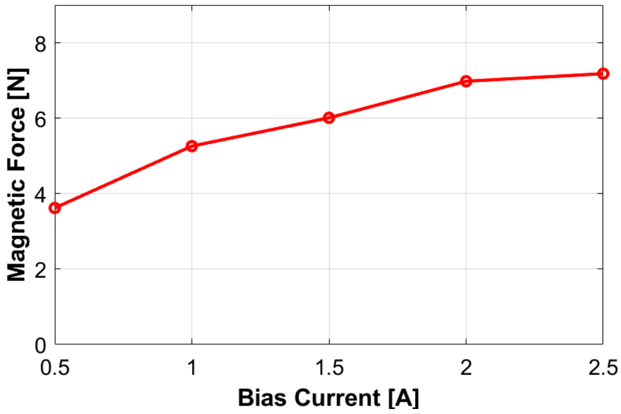

Figure 6. Magnetic force vs. bias current

As for the power losses (Fig. 7), both the ohmic and the iron components increase when the bias current is higher, which is also indicated by Equations (7) and (8) (higher coil current leads to higher magnetic flux density ***B***). Thus, for this specific parameter, it becomes clear that it should be quite larger than the maximum control currents in which the magnets will operate in order to enable more robust force control. However, very high values should be avoided due to the increase in losses and the possibility of approaching the saturation limit of the ferromagnetic materials. Of course, when dealing with electric current values, the power amplifier's limitations and the wire's capacity should also be considered. All the results from Figures 2 to 7 are summarised in Table 5.

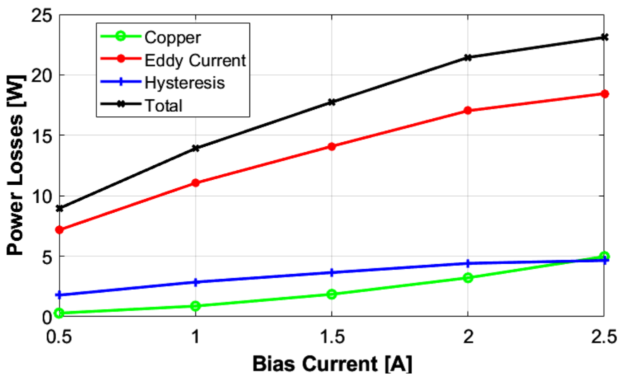

Figure 7. Power losses vs. bias current

3.2 Control current and power losses for constant mechanical load (Test 2)

For Test 2, a specific rotor load is assumed at 40 N. By keeping the bias current of the coils constant, several lengths and air gaps are tested, and the required control current for each case is calculated. Considering the ohmic and iron losses that occur each time, the optimum values of length and air gap are selected for this load, and significant conclusions are made regarding the effect of those two geometry parameters on the AMB's efficiency.

Table 5. Calculated magnetic forces and power losses (Test 1)

AMB's length, mm	Air gap, mm	Rotor's diameter, mm	Bias current, A	Magnetic force, N	Total loss, W
30.0	0.440	46.500	1.5	4.01	11.12
37.5				5.01	13.86
45.0				6.01	17.74
52.5				7.01	19.41
60.0				8.01	23.63
45.0	0.275	46.665	1.5	8.30	18.57
	0.330	46.610		7.39	18.19
	0.385	46.555		6.88	18.91
	0.440	46.500		6.01	17.74
	0.495	46.445		5.53	17.31
	0.550	46.390		5.20	18.04
	0.605	46.335		4.71	16.88
45.0	0.440	46.500	0.5	3.62	8.95
			1.0	5.26	13.91
			1.5	6.01	17.74
			2.0	6.98	21.44
			2.5	7.18	23.10

The control currents and the power losses calculated are summarised in Table 6. It is clear and well-expected that higher control currents are needed for smaller AMB lengths and bigger air gaps, as those geometries were proven to be the weakest in Test 1. This behaviour becomes clear in Figure 8, where the colour of the 2D curve when blue, indicates the lowest control current values needed while when being red indicates the highest ones. This curve has a homogenous and consistent behaviour that is easy to interpret.

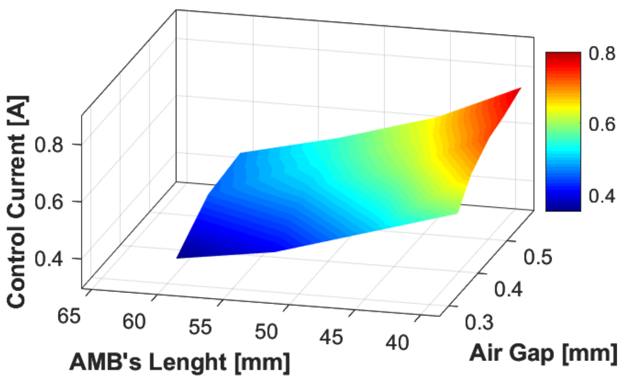

Figure 8. Control current required for 40 N of mechanical load in several cases

Table 6. Calculated control currents and power losses (Test 2)

Air gap, mm	Rotor's diameter, mm	AMB's length, mm	Control current, A	Iron loss, W	Ohmic loss, W	Total loss, W
0.33	46.61	37.5	0.6	35.10	4.20	39.30
		45	0.5	40.83	4.38	45.21
		52.5	0.4	42.95	4.57	47.52
		60	0.35	48.42	4.85	53.27
0.385	46.555	37.5	0.7	34.81	4.43	39.24
		45	0.55	40.32	4.49	44.81
		52.5	0.45	49.66	4.66	54.32
		60	0.4	56.00	4.94	60.94
0.44	46.5	37.5	0.75	35.16	4.56	39.72
		45	0.6	43.84	4.60	48.44
		52.5	0.5	46.54	4.76	51.30
		60	0.45	52.67	5.03	57.70
0.495	46.445	37.5	0.77	37.72	4.62	42.34
		45	0.63	40.83	4.67	45.50
		52.5	0.53	46.60	4.83	51.43
		60	0.46	56.49	5.05	61.54
0.55	46.39	37.5	0.8	34.30	4.70	39.00
		45	0.65	42.20	4.72	46.92
		52.5	0.55	47.77	4.87	52.64
		60	0.47	49.48	5.07	54.55

Figure 9 presents the behaviour of power losses for all the calculated cases as a graph. The effect of the AMB's length is clear; smaller lengths are more efficient since they support the same load with significantly lower power loss, despite the fact that the control currents needed are higher. The air gap on the other side does not seem to have a specific effect, mostly being the reason for the ruffle shape of the curve. While higher currents increase the ohmic component of the losses, the iron loss component is less predictable. The flux density is affected negatively because of the air gap and positively because of the increase in electric current. The relationship between electric current and magnetic flux is nonlinear. The flux leakage caused by the bigger air gaps and the inhomogeneous distribution of the flux caused by the rotor's motion are the reasons for this behaviour. The optimum set of values in this analysis, as presented in Table 6, is a length of 37.5 mm and an air gap of 0.55 mm, resulting in 39 W of total loss. At the same time, the maximum loss (61.54 W) was noticed at a 60 mm length and 0.495 mm air gap. While this specific length value was the one with the lowest loss by far, the air gap value did not seem to play such a significant role in the losses.

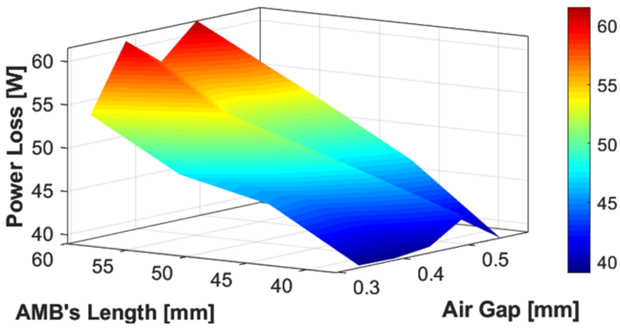

Figure 9. Power losses occurring in several cases for 40 N of mechanical load

4. Conclusion

When it comes to the power losses of an AMB system, it seems that each of the tested parameters, AMB's length, the air gap and bias current plays its own role. Whether its effect is important or not, it can be verified only by accounting for the mechanical load of the AMB, which is the main required outcome of such a system.

In the two tests carried out in this analysis, the power losses of an AMB were addressed, as well as its mechanical load capacity, in relation to the bias current, the length and the magnetic air gap. While the air gap does not show a consistent behaviour regarding the power loss, at least for the selected value range, the bias current and the length provided some solid conclusions. Increasing the bearing's length while keeping the current constant enables the support of higher mechanical loads but also increases the power loss. Equivalently, the same load can be carried with a longer AMB by applying lower currents on its coils compared to a shorter one. However, the solution of higher currents in a shorter bearing is more efficient. When it comes to bias currents, they need to be higher than the control currents but not too high, as losses will increase significantly. Very low values, on the other hand, might cause some magnets to have near-zero flux. As a result, this will affect the magnetisation of the rotor while rotating, leading to a magnetic force lower than expected. Additionally, control currents should always be lower than bias currents because the magnetic flux's direction in each of the "circuits" created between the stator's poles and the rotor should remain constant.

While the FEM model used in this analysis has been validated using results already published in the literature, an experimental approach of the same tests would be useful. A further expansion of the model could be attempted to include the rotor's dynamic behaviour. This behaviour would be the source of additional losses due to the alternating control currents needed to suppress the dynamic loads. Apart from the mechanical part, the electronic part, i.e. the switching power amplifier, could be simulated. The current ripples occurring from the pulse-width modulators also play a role in the system losses. However, even if the results do not include some of the losses that would appear in a real-case scenario, they give an accurate picture regarding the behaviour of the losses and the magnetic force when geometry and operational parameters change. Having sufficient FEM models that can quantify and handle each one of the problem's conflicting parameters could be beneficial to a design optimisation process as well, as they could be the main source of data for a machine learning algorithm, thanks to their flexibility and computational efficiency.

Acknowledgement

The present work was financially supported by the "Andreas Mentzelopoulos Foundation".

References

[1] M. Gärtner, C. Brecher, S. Neus, L. Catana, F. Greco, G. Morales-Espejel, D. Lang, Evaluation of hybrid spindle bearings with nitriding raceway steels under high rotational speeds, Tribology and Materials, Vol. 2, No. 3, 2023, pp. 88-98, DOI: 10.46793/tribomat.2023.012

[2] B.A. Abass, M.A. Mahdi, Effect of microridges on the performance of three-lobe journal bearing considering cavitation and lubricant compressibility, Tribology and Materials, Vol. 2, No. 4, 2023, pp. 189-200, DOI: 10.46793/tribomat.2023.016

[3] E.H. Maslen, G. Schweitzer (Eds.), Magnetic Bearings, Springer, Berlin, 2009, DOI: 10.1007/978-3-642-00497-1

[4] C.R. Knospe, Active magnetic bearings for machining applications, Control Engineering Practice, Vol. 15, No. 3, 2007, pp. 307-313, DOI: 10.1016/j.conengprac.2005.12.002

[5] Z. Wang, C. Zhu, Active control of active magnetic bearings for maglev flywheel rotor system based on sliding mode control, in Proceedings of the 2016 IEEE Vehicle Power and Propulsion Conference (VPPC), 17-20.10.2016, Hangzhou, China, DOI: 10.1109/VPPC.2016.7791603

[6] X. Ren, Y. Le, B. Han, K. Wang, Loss optimization and thermal analysis of a heteropolar magnetic bearing for a vacuum turbo-molecular pump, International Journal of Applied Electromagnetics and Mechanics, Vol. 54, No. 4, 2017, pp. 673-690, DOI: 10.3233/JAE-170009

[7] T. Huang, M. Zheng, G. Zhang, A review of active magnetic bearing control technology, in Proceedings of the 2019 Chinese Control And Decision Conference (CCDC), 03-05.06.2019, Nanchang, China, pp. 2888-2893, DOI: 10.1109/CCDC.2019.8833062

[8] Y. Le, K. Wang, Design and optimization method of magnetic bearing for high-speed motor considering eddy current effects, IEEE/ASME Transactions on Mechatronics, Vol. 21, No. 4, 2016, pp. 2061-2072, DOI: DOI: 10.1109/TMECH.2016.2569822

[9] Z. Xu, H. Zan, H. Bangcheng, Z. Yiming, Y. Xiangyang, Iron loss prediction model for radial magnetic bearing of molecular pump considering temperature influence, in Proceedings of the 2018 21st International Conference on Electrical Machines and Systems (ICEMS), 07-10.10.2018, Jeju, South Korea, DOI: 10.23919/ICEMS.2018.8549213

[10] X. Zhang, B. Han, X. Liu, Y. Chen, L. Zhai, Prediction and experiment of DC-bias iron loss in radial magnetic bearing for a small scale turbomolecular pump, Vacuum, Vol. 163, 2019, pp. 224-235, DOI: 10.1016/j.vacuum.2019.02.012

[11] B. Han, Z. He, X. Zhang, X. Liu, T. Wen, S. Zheng, Loss estimation, thermal analysis, and measurement of a large-scale turbomolecular pump with active magnetic bearings, IET Electric Power Applications, Vol. 14, No. 7, 2020, pp. 1283-1290, DOI: 10.1049/iet-epa.2020.0037

[12] R. Siva Srinivas, R. Tiwari, C. Kannababu, Application of active magnetic bearings in flexible rotordynamic systems – A state-of-the-art review, Mechanical Systems and Signal Processing, Vol. 106, 2018, pp. 537-572, DOI: 10.1016/j.ymssp.2018.01.010

[13] O.W. Taha, Y. Hu, Modeling of a digital twin for magnetic bearings, Applied Sciences, Vol. 13, No. 14, 2023, Paper 8534, DOI: 10.3390/app13148534

[14] Y. Hu, O.W. Taha, K. Yang, Fault detection in active magnetic bearings using digital twin technology, Applied Sciences, Vol. 14, No. 4, 2024, Paper 1384, DOI: 10.3390/app14041384

[15] T. Santra, D. Roy, A.B. Choudhury, S. Yamada, Multiphysics modelling of a hybrid magnetic bearing (HMB) for calculating power loss and temperature with different loss minimization strategies, Tribologia, Vol. 36, No. 1-2, 2019, pp. 24-35, DOI: 10.30678/fjt.60402

[16] V.-M. Koufopanos, P.G. Nikolakopoulos, Finite element simulation of iron losses for an active magnetic bearing-rotor system constructed of Hiperco laminations, Simulation Modelling Practice and Theory, Vol. 135, 2024, Paper 102956, DOI: 10.1016/j.simpat.2024.102956

[17] K. Li, Z. Deng, C. Peng, G. Pang, L. Mei, C. Yu, Mechanism analysis of eddy-current effects on switching power amplifier of a nonlaminated magnetic bearing, IEEE Access, Vol. 8, 2020, pp. 147112-147121, DOI: 10.1109/ACCESS.2020.3015502

[18] S. Shelke, R.V. Chalam, Optimum energy loss in electro magnetic bearing, in Proceedings of the 2011 3rd International Conference on Electronics Computer Technology, Vol. 3, 08-10.04.2011, Kanyakumari, India, pp. 374-379, DOI: 10.1109/ICECTECH.2011.5941775

[19] C. Yu, Z. Deng, L. Mei, C. Peng, X. Cao, Multiobjective optimization of 3-DOF magnetic bearing considering eddy current effects and saturation, Mechanical Systems and Signal Processing, Vol. 182, 2023, Paper 109538, DOI: 10.1016/j.ymssp.2022.109538

[20] Y. Zhang, J. Tang, X. Xu, Z. Huang, Optimal design of magnetically suspended high-speed rotor in turbo-molecular pump, Vacuum, Vol. 193, 2021, Paper 110510, DOI: 10.1016/j.vacuum.2021.110510

[21] K.P. Lijesh, H. Hirani, Optimization of eight pole radial active magnetic bearing, Journal of Tribology, Vol. 137, No. 2, 2015, Paper 024502, DOI: 10.1115/1.4029073

[22] D. Rodriguez-Sotelo, M.A. Rodriguez-Licea, I. Araujo-Vargas, J. Prado-Olivarez, A.-I. Barranco-Gutiérrez, F.J. Perez-Pinal, Power losses models for magnetic cores: A review, Micromachines, Vol. 13, No. 3, 2022, Paper 418, DOI: 10.3390/mi13030418

[23] S. Saha, Mashuq-un-Nabi, A review on active magnetic bearing and exploitation of parametric model order reduction, in Proceedings of the 2016 11th International Conference on Industrial and Information Systems (ICIIS), 03-04.12.2016, Roorkee, India, pp. 420-425, DOI: 10.1109/ICIINFS.2016.8262977

[24] Silicon Core Iron B, available at: https://www.carpentertechnology.com/alloy-finder/silicon-core-iron-b, accessed: 10.07.2024.

[25] G. Bertotti, General properties of power losses in soft ferromagnetic materials, IEEE Transactions on Magnetics, Vol. 24, No. 1, 1988, pp. 621-630, DOI: 10.1109/20.43994

[26] Ansys® Electronics Suite, Release 19.2, Maxwell Help, Specifying the Solver Type Guide, Ansys, Inc.

[27] B.S. Guru, H.R. Hiziroğlu, Electromagnetic field theory fundamentals, Cambridge University Press, Cambridge, 2004, DOI: 10.1017/CBO9781139165297